RSC Advances

ROYAL SOCIETY OF CHEMISTRY

www.rsc.org/advances

Journal Name

ARTICLE

Rectangular ZnO porous nano-plate assembly with excellent acetone sensing performance and catalytic activity

Received 00th January 20xx,
Accepted 00th January 20xx

DOI: 10.1039/x0xx00000x

www.rsc.org/

Arnab Kanti Giri,[a] Arka Saha,[a] Aniruddha Mondal,[a] Subhash Chandra Ghosh,[a] Susmita Kundu,[b,*] Asit Baran Panda [a,*]

Controlled synthesis of hierarchically assembled porous rectangular ZnO plate (2.5-3.5µm length, 1.5 -2.5µm width and 100-150nm thickness) from bulk ZnO without using any organic substrate such as solvent /surfactant /structure-directing agent is presented. Synthesized ZnO plates are single crystalline with exposed (10$\bar{1}$0) facet in flat surface, porous and formed through the calcination of hydrozincite [$Zn_5(CO_3)_2(OH)_6$] intermediate. The gas sensor based on the synthesized porous ZnO architecture exhibited high sensitivity towards acetone even in low concentration (S=3.4 in 1 ppm acetone) with good selectivity. The ZnO nanostructure material as heterogeneous catalyst also showed excellent catalytic activity for the synthesis of 5-substituted-1H-tetrazoles (yield = 94%). Both the activities are superior than that of other reported ZnO based acetone sensors and heterogeneous catalyst. We belive that, the improved properties of synthesized ZnO nanostructure is due to the exposed (10$\bar{1}$0) facet, porous and assembled structure, which provides reasonably large accusable surface area, facilitate diffusion and mass transport of gas or substrate molecules.

Introduction

Owing to the cheap, abundant and unique optoelectronic properties Zinc oxide (ZnO), most important n-type semiconductors with a wide band gap of 3.37 eV and large exciton binding energy of ~60 meV, has been investigated extensively.[1] ZnO finds tremendous technological application in different fields, including as sensor and as heterogeneous catalyst.[1-3] It is well-known that the properties of ZnO is highly controlled by its size, shape and morphology.[4-11] Among the developed shapes,[5-11] uniform ZnO plates are most important and showed enhanced properties over other shapes, specifically to that of rod, due to their 2D structure, high surface area and presence of active facets in the flat surface.[12] The applications like sensor, catalysis, energy conversion and storage, where accessible surface is more important, the 3D hierarchical assembly of these 2D plates are highly desirable, compare to that of stacked one.[13] They provides improved and novel properties and probability of gradual reduction of property originating from the decrease in accessible surface area can be avoided. These 3D hierarchical structures also offer the opportunity to study the structure–property relations as well as diverse material fabrication techniques.[14-15] Furthermore, porosity in these individual 2D plates makes them key important materials specifically for the above mentioned applications, as these porous structures offer negligible diffusion rate and favourable kinetics for enhanced properties, and *in-turn* showed improved properties.[9-11]

Although, number of reports are there on assembled or non-assembled 2D irregular ZnO nano-plate/sheets, without any specific dimensions,[6-11] but the reports of uniform porous ZnO plates with specific dimension, like hexagonal/ rectangular shape, are very limited. Liu *et al*.[16] and Wan *et al.* [17] reported hexagonal ZnO plates through decomposition of ZnS(en)0.5 and ammonium zinc nitrate, respectively and they have used hazardous ethylenediamine and poly (styrene euphonic acid) as structure directing agent to get the uniform plate structure. Reeja-jayan *et al.* [18] reported spongy ZnO disk in ethanol, with very low yield and most of these reported plates are not assembled. To best of our knowledge, there are no reports on synthesis of porous and uniform ZnO plates, and their 3D assembly. Thus, it is highly desirable and challenging to develop a suitable and convenient route for assembled uniform porous plate.

Synthesis of porous ZnO nanostructure through hydrozincite [$Zn_5(CO_3)_2(OH)_6$] intermediate is one of the most important method.[9-11] During calcination of carbonate intermediate, a large amount of CO_2 and H_2O is evolved and generated a reasonable amount of pores in the structure. However, most of these methods frequently used hazardous organic substrates as structure and/or pore directing agent and commonly crystallize in random as well as assembled irregular sheet structures.[9-11]

[a] Discipline of Inorganic Materials and Catalysis, and Academy of Scientific and Innovative Research, CSIR-Central Salt and Marine Chemicals Research Institute, G.B. Marg, Bhavnagar-364002, Gujarat, India..
[b] Sensors and Actuators division, CSIR-Central Glass & Ceramic Research Institute, Kolkata-700032, West Bengal, India.
Electronic Supplementary Information (ESI) available: [XRD, TG-DTG and IR of hydrozincite, magnified TEM & SEM image, Catalytic activity results]. See DOI: 10.1039/x0xx00000x

Herein, *first time,* we report the synthesis of stable 3D hierarchically assembled porous uniform rectangular ZnO plate (2.5-3.5µm length, 1.5 -2.5µm width and 100-150nm thickness) through calcination of corresponding rectangular hydrozincite intermediate, without using any organic additives. The obtained individual ZnO plates are single-crystalline. Hydrozincite intermediate was synthesized by a novel hydrothermal method using bulk ZnO and aqueous ammonium carbonate solution. The use of bulk ZnO makes the procedure attractive and advantageous. A tentative formation mechanism of such assembled plate mediated hydrozincite morphologies as well as porous ZnO is discussed based on the experimental results and crystallographic point of view. In the present study, we have explored the acetone sensing properties of the synthesized ZnO nanostructure and showed superior sensing performance, with quite high selectivity, even at 1 ppm acetone vapour. The catalytic activity of the synthesized porous ZnO nanostructure has also been explored for the synthesis of 5-substituted-1H-tetrazole derivatives. Both the catalytic and sensing activity is better than that of reported results.

Experimental

Chemicals.

Analytical grade bulk zinc oxide (ZnO) was procured from Rankem (Ranbaxy), India; ammonium carbonate (NH_4HCO_3 and $NH_2CO_2NH_4$, 95.3%), were purchased from Marck, India. All the chemicals were used as-obtained without any further purification. Water with a resistivity of 18 MΩ cm^{-1}, obtained from a Millipore water purifier, was used for all the performed experiment.

Synthesis of 3D assembled ZnO from their corresponding hydrozincite intermediate

In a typical procedure, to a 0.5 g of bulk ZnO dispersed in 20 mL of water 2.3 g of solid ammonium carbonate was added with continuous stirring (500 rpm). Within 2–3 min the solution became clear. Then, 40 ml of water was added to the clear solution and stirred (500 rpm) for 5 min. 33 ml of the resultant solution was transferred to 50ml Teflon lined stainless steel autoclave and kept in a pre-heated oven at 200°C for 20h. The resultant white materials were collected through centrifugation and washed with water for several times. The materials were dried at 70–80 °C for 12 h. The dried intermediate was calcined in the temperature range of 400-600°C for 2 h to obtain desired ZnO.

Characterizations.

Powder X-ray diffraction patterns of the samples were obtained using a Rigaku MINIFLEX-II (FD 41521) powder diffractometer. The thermo-gravimetric analysis of the synthesized hydrozincite was performed using a Mettler-Toledo (TGA/SDTA 851e) instrument. The nitrogen sorption measurements were carried out using an ASAP 2020 Micromeritics, USA. To determine the morphology of the samples, Scanning electron micrographs (SEM) and field emission - Scanning electron micrographs (FE-SEM) were obtained using a Leo series 1430 VP and ZEISS SUORA 35 VP scanning electron microscope, respectively. Transmission electronic microscopy (TEM) images of the synthesized ZnO were recorded using a JEOL JEM 2100 microscope. The FT-IR spectra were recorded with a Perkin-Elmer GX spectrophotometer in the range 400–4000 cm^{-1} using a KBr pellet. Diffuse reflectance spectra (DRS) of ZnO and doped ZnO samples were obtained using a Shimadzu UV-2550 spectrophotometer. The detailed procedures for characterizations were described in the papers previously published by us.[3]

Sensing Experiment

The synthesized ZnO samples were mixed with a suitable amount of isopropanol to form a paste. The paste was then coated onto alumina tubes on which two gold electrodes and platinum wires were placed at each end (coating thickness ~ 100 µm). The gold electrode and platinum lead wires were attached to the end of the tubes by curing the system at a high temperature before applying the paste. [19] The coated alumina tubes were cured at 500°C for 30 min.

The electrical resistance, gas response as well as recovery and response times of the sensors were measured in the temperature range of 200 to 400°C in an ambience of ~ 50 % relative humidity by using a digital multimeter (Agilent U1252A) and a constant voltage/current source (Keithley 228A). The sensors to be measured were placed in the bottom of a quartz tube (2 cm diameter and 10 cm length and volume ~ 30 cm^3) and externally connected through a digital multimeter and a constant voltage/current source to record the sensor resistance. The sensors were exposed to very low concentration (0.5 to 100 ppm) of acetone vapor, made within desiccators by serial dilution method as given elsewhere (For details of the preparation of 0.5-1 ppm acetone through serial dilution method please see Supporting Information).[20] The cross sensitivity of some specific sensors were also checked in CO, n-butane gases, ethanol vapor and in saturated moisture. The response S is defined as:

$$S = R_a/R_g \quad \ldots\ldots(1)$$

where R_a is the sensor resistance in air at the operating temperature, and R_g is the sensor resistance in the vapour at the same temperature. The detailed assembly of fabricated sensor and corresponding calculation has been presented in ESI†and Fig. S1, and also described elsewhere.

Catalytic activity Study.

Synthesized ZnO nanostructure was used as catalyst for the synthesis of 5-substituted 1H-tetrazole. In a typical procedure, 2.5 mmol benzonitrile, 2.75 mmol (1.1 eq) sodium azide and 3 mL DMF as a solvent were taken in a 25 ml RBF. To that mixture 0.1 g ZnO was added, and the reaction mixture was heated at 125 °C for 14 h under constant stirring (700 rpm). Progress of the reaction was monitored by TLC (thin-layer chromatography). After completion of the reaction, 20 ml ethyl acetate was added to reaction mixture, catalyst was separated by filtration and thefiltrate was washed with

distilled water (3x20 mL). During washing 20 mL 3N HCl was added to the organic layer under vigorous stirring and the organic layer was separated. The aqueous layer was re-extracted with ethyl acetate for 3 times. The all the organic layers were collected, again washed with water and dried over anhydrous sodium sulfate. After evaporation of solvent in vacuo, the solid crystalline tetrazole was obtained and purified by re-crystallization. Synthesized different tetrazoles were characterized by 1H and 13C NMR, FT-IR, and CHN analysis (see ESI†).

Results and discussions

Synthesis and characterization

The established strategy for the synthesis of 3D assembled uniform porous single-crystalline rectangular ZnO plates is based on the formation of corresponding hydrozincite plates, through *in-situ* dissolution of bulk ZnO and formation of zinc carbonate in presence of ammonium carbonate by the formation of zinc ammonium carbonate complex, followed by calcination. The bulk ZnO was used to make the procedure more economical and useful.

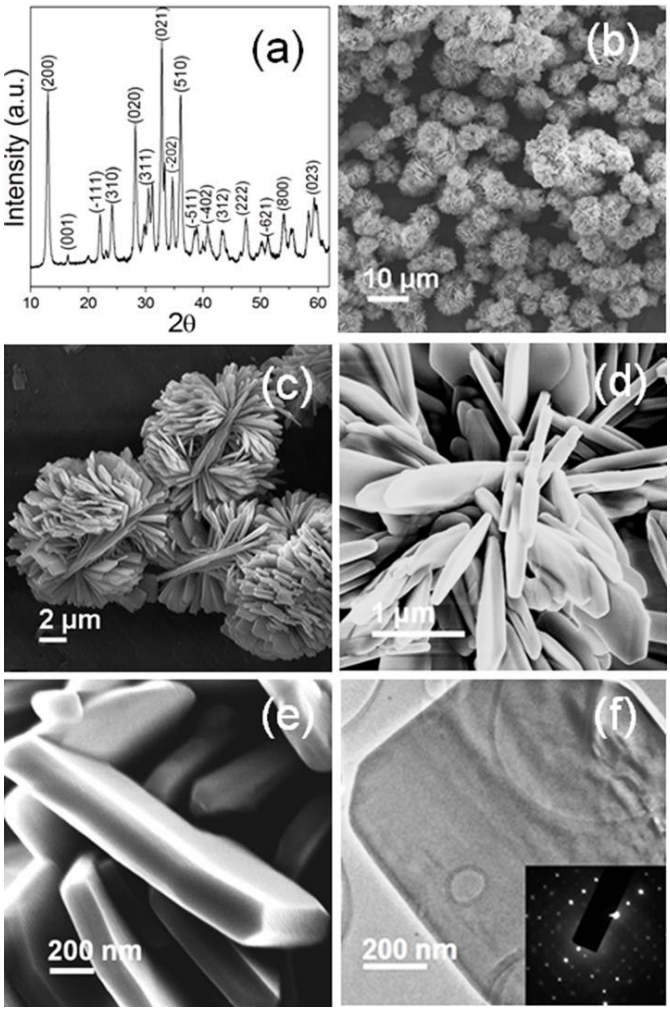

Fig. 1 (a) XRD pattern, (b-e) SEM and FE-SEM images, and (f) TEM image of synthesized rectangular hydrozincite intermediate.

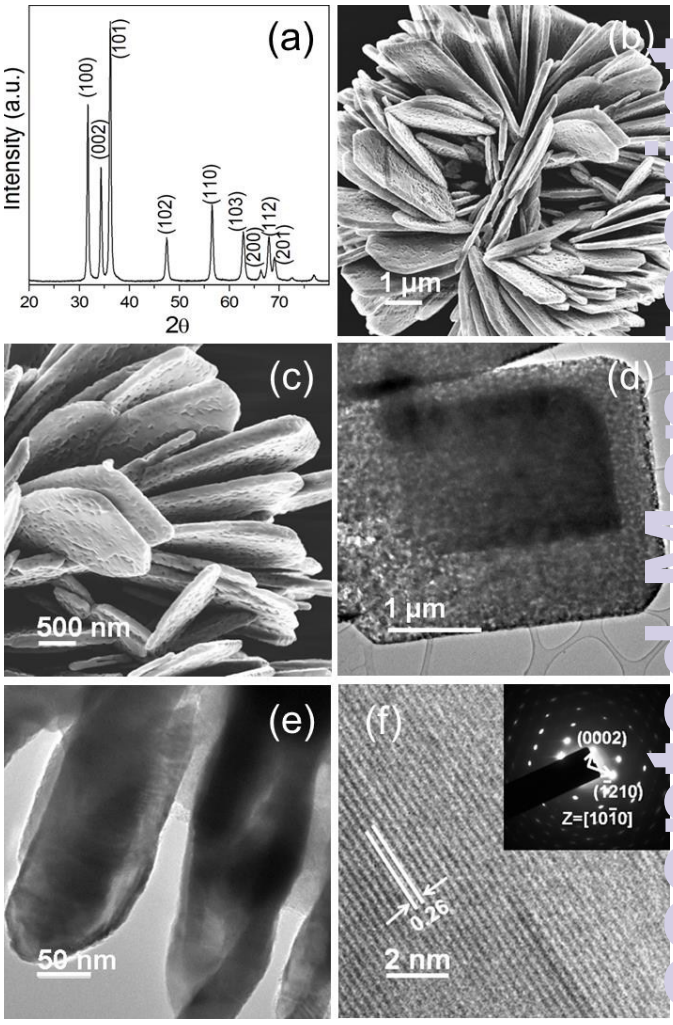

Fig. 2 (a) XRD pattern, (b-c) SEM and FE-SEM images, and (d-f) TEM image of assembled rectangular ZnO nanoplates synthesized through calcination of hydrozincite intermediate at 500 °C for 2 h.

All the diffraction peaks in XRD pattern of as-synthesized carbonate intermediate can be indexed to the monoclinic hydrozincite phase [$(Zn_5(CO_3)_2(OH)_6)$, JCPDS card no. 19-1458] and absence of any additional peak, other than hydrozincite, confirmed the formation of phase pure hydrozincite (Fig. 1a). In the TG analysis curve, the 27.5 % weight loss in second stage in temperature 200–475°C, assigned to the removal of H_2O and CO_2 due to the decomposition of hydrozincite to ZnO, is very close to that of theoretical weight loss (26.2%) of hydrozincite and confirmed that intermediate is nothing but hydrozincite. No distinct weight loss after 475°C indicate the total decomposition of hydrozincite intermediate to ZnO (Fig. S2, ESI†). FT-IR spectra of bare and calcined materials also support the conversion of hydrozincite to ZnO (Fig. S3, ESI†). Low-magnified SEM image (Fig. 1b-c) of hydrozincite intermediate evidenced the formation of uniform 3D assembly of plates. Higher-magnified SEM and FE-SEM images indicate that it is nothing but a 3D assembly of uniform rectangular plates of smooth surface with ~2.5-3.5µm length, 1.5 -2.5µm width and 100-150nm thick (Fig. 1d-e). TEM images of the hydrozincite also confirmed the formation of assembled

rectangular plates with uniform size. Corresponding selected area electron diffraction (SAED) pattern confirms that the hydrozincite plates are single crystalline with (100) plane for the planer surface (Fig. 1f).

The XED pattern of the carbonate intermediate calcined at 500°C exhibit well resolved diffraction peaks, can be indexed to the planes of hexagonal wurtzite structure of ZnO (space group *p63mc*, JCPDS 36-1451) and confirmed the formation of phase pure ZnO (Fig. 2a). The average crystallite size of the calcined samples, calculated from X-ray line broadening of all individual diffractions using Scherrer's equation, were found ~18 nm. Fig. 2b-c represents the FE-SEM of the calcined ZnO and evidenced that no noticeable morphological change took place on calcination. However, the surface of the plates became rough on calcination, most probably due to the generation of pores in the plates for the evolution of generated CO_2 and H_2O during decomposition of hydrozincite intermediate. Corresponding TEM image showed the 3D assembly of plates (Fig. S4, ESI†). TEM image of individual plate through flat surface evidenced the plates are rectangular with ~2.5µm length, 1.5 µm width and highly porous in nature (Fig. 2d). TEM Image of vertically aligned plates depicts the thickness of the plates, which is ~130nm (Fig. 2e). All the TEM observations also support the SEM observations. Magnified images also further confirmed the porous nature of plates with a pore size in the range of 40–50 nm (Fig. S5, ESI†). The well resolved distinct lattice fringes through-out the plates in the HR-TEM image further confirmed that the plates are highly crystalline in nature. The inter-planer distances of 0.26 nm can be indexed to d-spacing of (002) plane of hexagonal wurtzite ZnO and supports the XRD results (Fig. 2f). The SAED pattern focused on flat surface of plate consist of well-ordered dots, indexed to (0002) and ($\bar{1}$210) planes of hexagonal ZnO and depict the synthesized rectangular ZnO plates are single

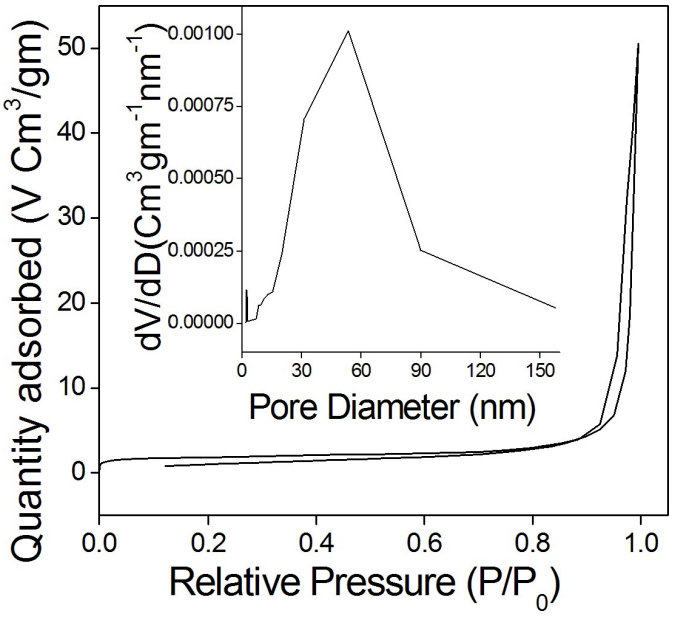

Fig. 3 The nitrogen sorption isotherm and corresponding pore size distribution curve (inset) of the synthesized porous rectangular plate assembled ZnO architecture calcination at 500 °C for 2 h.

crystalline in nature (inset Fig. 2f). From the TEM and SAED pattern, it is well understood that the planer surface of synthesized ZnO is of (10$\bar{1}$0) surface.

Textural properties and corresponding inner architectures of the pores in the synthesized 3D assembled rectangular porous ZnO plates were obtained from nitrogen sorption experiments. Surface area measurement experiments were performed in the pressure range of 0.05 to 1.0. The sorption isotherm in the pressure range were found to be type II (according to the IUPAC classification) and the hysteresis loop can be ascribed to the type H3 (Fig. 3). A broad pore size distribution was observed, calculated using the BJH method from the adsorption part of the isotherm. Synthesized ZnO plates contain the pores in the size range of 30-70 nm, predominantly and support the TEM observation. The BET surface area of the synthesized ZnO plates calcined at 500 °C was calculated to be 24 m^2g^{-1} and was decreased on increase in temperature (Table S1).

ZnO is frequently used as a UV filter. Thus, DRS measurement of the synthesized assembled ZnO plates was also performed. The DRS of synthesized ZnO as well as bulk ZnO showed almost identical spectra but for the synthesized ZnO architectures very little shifting of band edge towards blue reason with respect to corresponding bulk was observed (Fig. S6, ESI†). However, this minute shifting is unusual as the particle size of the synthesized ZnO is quite high, which is nothing but the single crystalline pore wall thickness, than that of its Bohr radius. This is most probably due to the presence of very thin bridge between the synthesized nanostructures.

Formation Mechanism

To understand the stepwise formation mechanism, a series of experiments were performed by changing the reaction parameters like time, temperature and amount of ammonium carbonate. After the addition of ammonium carbonate to bulk ZnO with constant stirring at room temperature, within 1-2 min it results a clear solution of ammonium carbonate complex. But, its stability is very less, within another 2-3 min, the solution became turbid by forming the zinc hydroxyl carbonate as precipitate,[3, 9d] which on hydrothermal treatment (200°C/24h) gave the desired 3D assembly of plates. SEM images of the intermediate, obtained after 2h of hydrothermal treatment, depict the formation of random sheets (Fig. 4a). In 4h, it resulted the stacking of elongated sheets towards sheaf-like structures (Fig. 4b). The shape of the materials were further changed into sheet assembled dumbbell like structures by forming additional sheets in the edges of sheaf-like structures upon hydrothermal treatment for 8h and with increase in time the density of sheet in two side increased gradually (Fig. 4c-f). In initial stage, the thickness of the flake was very thin and the side walls were rough, i.e., steps and kinks. However, with the increase in the hydrothermal treatment time the plates were arranged closely, widths of the plates were reduced, thickness was increased gradually, side walls were became smooth and resulted exact rectangular shape (Fig. 4c-f). After 24h no such further morphological change was observed. Hydrothermal treatment temperature

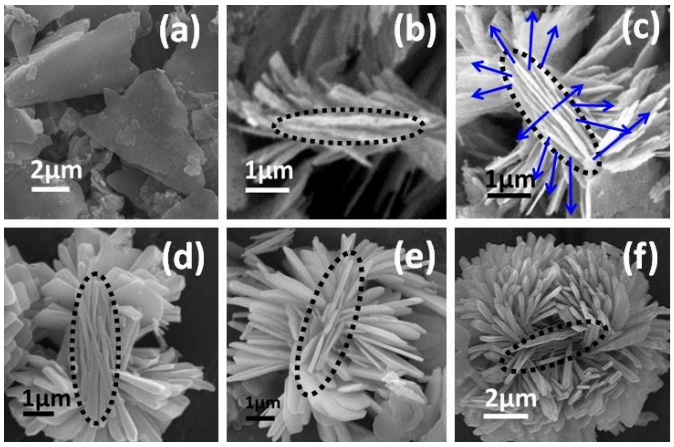

Fig. 4 SEM images of intermediates formed during hydrothermal treatment of the resultant aqueous solution of bulk ZnO and ammonium carbonate at 200°C (a) after 2h, (b) after 4h, (c) after 8h, and (d) after 12h (e) after 16h and (f) after 24h.

also has distinct effect on the formation of rectangular plates and their assembly. In 125 °C and 150 °C, it was resulted 3D assembly of thin flakes even after 24h of hydrothermal treatment (Fig. S7a-b, ESI). A 3D assembly of mixed rectangular plates and thin sheet was produced in 175 °C (Fig. S7c, ESI). Whereas at higher temperature (225°C), it resulted thick, thicker than the product at 200°C, rectangular plates with short range ordering of plates (Fig. S7d, ESI). Here it is important to mentioned that the amount of carbonate don't have any significant effect on morphology, 1.8 g ammonium carbonate for 0.5 g bulk ZnO, minimum amount required to dissolve ZnO.

In general, formation of a specific morphology and there phase transformation is controlled by the Gibbs-Curie-Wulff theorem.[21] Thus, in the initial stage of reaction, the crystalline phase of seed is the key factor of growth and corresponding morphology, which governs the intrinsic shape originating from the corresponding symmetry of the structure.[21] The reaction condition also has prime role in the morphology of the final product, by controlling the growth through specific facet of crystals, Ostwald ripening, oriented attachment etc. In the present reaction condition, aqueous ammonium carbonates dissociate to NH_4OH and H_2CO_3 and provide a basic condition. The bulk ZnO was hydroxylated to ammonium carbonate complex, under *in-situ* formed basic condition (equation in scheme 1).[3, 9d] Then the formed complex nucleates and crystallizes to monoclinic hydrozincite phase. Based on above mentioned time dependent SEM images, we propose 4 different growth stages of newly formed nuclei to final morphology. 1) In the first stage the hydrozincite nuclei is grown to commonly formed random thin sheet structure, with (100) plane for the planer surface (Fig. 1 & 4a); 2) then the individual shets splits to multiple sheets or secondary sheets were grown on the surface of the already formed sheet [22] and resulted the stacking of elongated sheets towards sheaf-like structures (Fig. 4b); 3) due to the highly branched sheets with high steps and kinks in side walls, the subsequent growth took place at the two heads of the stacked elongated sheets and

$$(NH_4)_2CO_3 + H_2O = NH_4^+ + H_2CO_3 + OH^- + NH_3$$
$$ZnO + 2OH^- + H_2O = Zn(OH)_4^{2-}$$
$$5Zn(OH)_4^{2-} + 2CO_3^{2-} = Zn_5(CO_3)_2(OH)_6 + 14OH^-$$
$$Zn_5(CO_3)_2(OH)_6 = 5\,ZnO + 3H_2O + 2\,CO_2$$

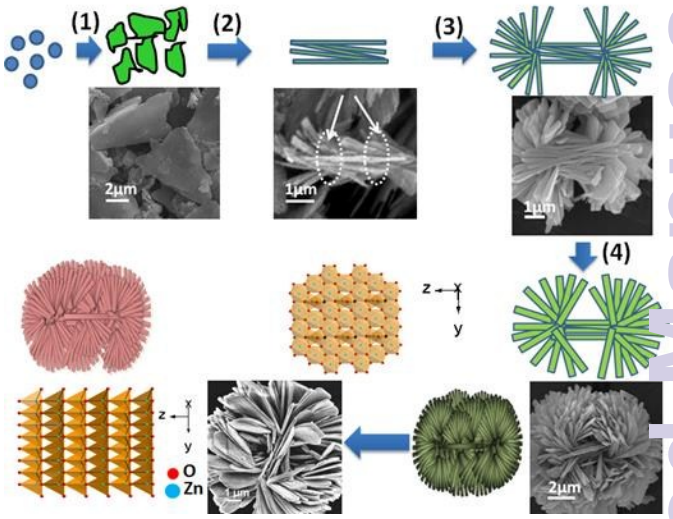

Scheme 1 Schematic representation of step wise reactio mechanism of assembled rectangular ZnO nanoplates. Upper panel: Probable chemical reaction; Lower panel: Step wise chance of shapes on with increase in hydrothermal treatment (1-4) and on calcination.

resulted the dumbbell like assembled sheet mediated morphology (Fig. 4c); 4) Under given hydrothermal condition (200°C), the sheet became thicker and resulted to rectangular shaped plate structure through Ostwald ripening (Fig. 4d). At low temperature (<180°C), it gave only thin flake, mo probably, the energy is not sufficient for Ostwald ripening. Whereas at higher temperature (>200°C) small and thicker rectangular plates were produced due to the enhanced Ostwald ripening process.

During calcination, the octahedral and tetrahedral unit of hydrozincite was collapsed by cleaving the Zn-O bond of Zn-O-C chains and dehydration between –OH groups. The structure collapse and bond cleavage generates CO_2 and H_2O. Thus, on escape of CO_2 and H_2O from the hydrozincite system number density of zinc was increased and resulted the topotactic transformation of original structure. Due to the topotactic transformation resulted contraction of original structure and generates huge void space. In the same time, formation of new Zn-O bonds of ZnO with tetrahedral structure took place. During phase transformation, the (100) crystal orientation of hydrozincite transformed to (100) orientation of hexagonal ZnO. Based on above discussions, a probable chemical reaction and pictorial step-wise formation mechanism is presented in Scheme 1.

Acetone sensitivity study

It is reported that hierarchically assembled poro s semiconductor metal oxides are the promising materials fo gas sensing applications.[7,10-11,15] It is very important to develo

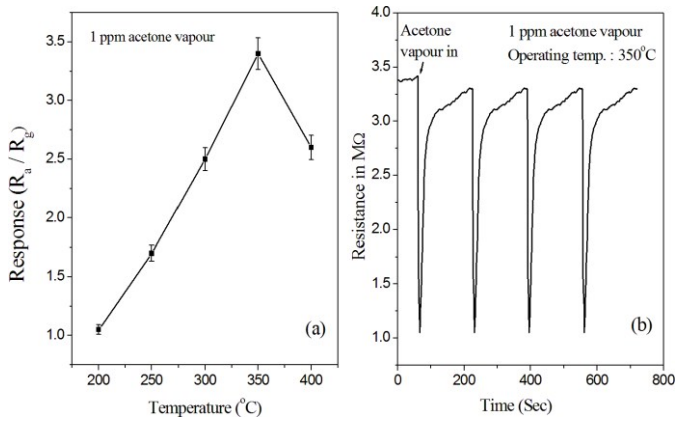

Fig. 5. (a) Response measured at different operating temperatures in presence of 1 ppm acetone vapor (b) corresponding change of base resistance at operating temperature of 350°C.

ZnO based acetone sensor with good sensitivity at low concentration, as ZnO is abundant and economical. Here, we have evaluated the acetone sensing property of synthesized ZnO architecture. It was observed that the ZnO calcined at 500°C showed superior sensing performance, and thus the detailed sensing study was performed using it.

Gas sensing response of semiconducting metal oxides, like ZnO, are highly influenced by the operating temperatures and concentration of gas. At low temperatures the sensor response is restricted due to low rate of diffusion of gas molecules and insufficient energy to react with the surface adsorbed oxygen species. With increase of temperature the rate of diffusion rate as well as surface reaction was gradually increased due to enhanced thermal energy. At higher temperature, although the energy was high enough to overcome the potential barrier of surface reaction but the rate of diffusion is too high to get the time to react in surface and *in-turn* the response decreased. Thus, a series of experiments were performed by varying the operating temperature, in the temperature range of 200 to 400°C, and concentration of acetone in the range of 1 to 100 ppm to evaluate the optimum conditions. Fig. 5a represents the sensitivity of synthesized ZnO exposed to 1

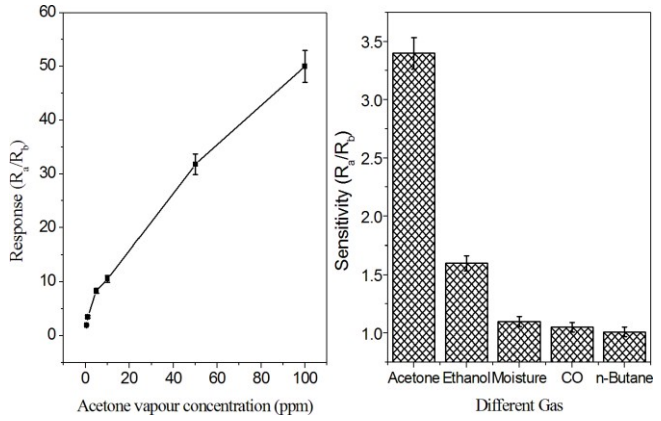

Fig. 6. Response of the sensor prepared using synthesized assembled ZnO plates in varying acetone concentration and (b) Response towards different gasses.

Table 1 Comparison of acetone sensing performance of ZnO nanostructure based sensor reported in literature with the synthesized assembled porous ZnO plates.

Material	Acetone conc.[a] (ppm)	Temp[b] (°C)	Response ($S=R_a/R_g$)	Ref.
Assembled ZnO plates	**1**	**350**	**3.4**	**This work**
	10	**350**	**10.6**	
	100	**350**	**50**	
Nestlike ZnO Hierarchy	100	420	17.4	11a
ZnO nanosheet	100	420	37.5	11b
ZnO nanosheet assembly	5	400	8.76	11c
ZnO sheet assembled flower	100	320	16.8	11d
Dumbbell like ZnO	50	300	16.0	11e
La2O3-ZnO rod	200	350	54.1	11f

[a] Concentration of acetone, [b] Operating temperature (°C)

ppm acetone at different temperature. It was observed that at 350 °C sensor shows the maximum sensitivity (S) of ~3.4, with response and recovery time of ~5 and ~20 s respectively. The corresponding change of base resistance in presence of 1 ppm acetone vapor is depicted in Fig. 5b. Fig. 6a represents the plot of sensitivity as a function of acetone concentration at an operating temperature of 350°C and evidenced that the synthesized ZnO has a wide detection range of acetone from 1ppm to 100ppm or more. As, in 1ppm the sensitivity is 3.4, so it is expected to sense acetone in ppb level also. Selectivity towards a particular gas is an important characteristic for a good sensor. Fig. 6b represents the selectivity study of synthesized ZnO as sensor in presence of different gases such as ethanol, CO, n-butane, as well as in saturated moisture. From the figure it is evident that the selectivity towards acetone is quite good. In 1ppm of ethanol the sensitivity is 1.6, whereas the sensitivity of other gases are very low.

The synthesized ZnO architecture showed reasonably good sensitivity and selectivity towards acetone at low concentration, as low as at 1 ppm with a sensitivity S= 3.4. In particular, the sensitivity response of the synthesized ZnO architecture is high and higher than those of reported pure and doped ZnO architectures.[10-11] Table 1 represents a comparison of sensing performance of synthesized ZnO architecture towards acetone with other reported pure and doped ZnO morphologies and confirmed the superior sensing performance towards acetone.

Catalytic activity study

Tetrazoles are one of the most important nitrogen-rich hetero-aromatic compounds with increasing popular functionalityfinds wide range of applications in pharmaceuticals, biomedical applications, agriculture, as anti-foggants in photographic materials, propellants and specialty explosives.[23] Generally, the 5-substituted-1H-tetrazoles are synthesized [3+2] cyclo-addition of azide to the corresponding nitriles in presence of hazardous Lewis acids, stoichiometric homogeneous catalysts; such as inorganic salts and metal complexes. Various heterogeneous catalysts has also been reported. However, the separation and recovery of homogeneous catalysts, use of large excess of poisonous azide (≥2:1), high reaction temperature and finally the poor yield are

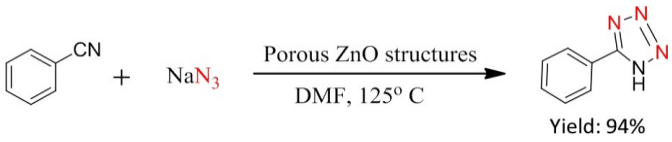

Scheme 2. Schematic representation of the synthesis of 5-phenyl-1H-tetrazole using the synthesized porous ZnO architecture as heterogeneous catalyst.

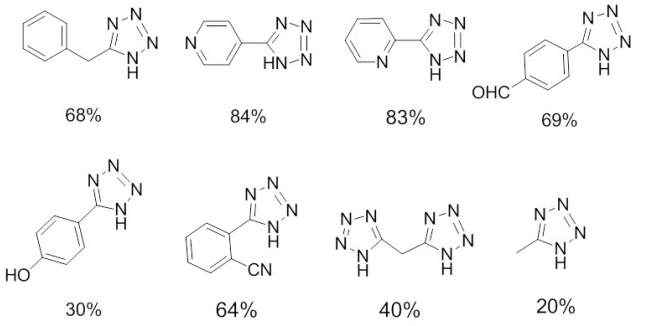

Fig. 7 Yield of tetrazoles compounds synthesized using the synthesized ZnO plates as catalyst.

the main drawbacks of most of the developed procedures. Thus, it is very important to develop a method with a reusable catalyst at low temperature for synthesis of 5-substituted-1H-tetrazoles using near stoichiometric amount of azide.

Thus, the synthesized hierarchically assembled porous ZnO rectangular plate architectures were utilized as heterogeneous catalyst for the synthesis of 5-phenyl-1H-tetrazole (Scheme 2) using benzonitrile and NaN_3 (with reduced amount, only a 1.1 molar ratio instead of literature reported 1:2) as reactant and DMF as solvent. The reaction was ended with single product of 5-phenyl-1H-tetrazole with the isolated yield of 94% at a reaction temperature of 125°C just in 14 h. The synthesized porous ZnO architecture showed superior catalytic activity over other reported heterogeneous catalyst, even the catalytic activity is comparable, sometime superior, with the homogeneous catalyst (Table S2, ESI†). Catalyst is reusable for several times and after 5th cycle the yield is 86% (Fig. S8 & S9-13). Then substrate scope was explored with our developed catalyst, and showed reasonably good catalytic activity towards other aliphatic and aromatic nitriles (Fig. 7).

Superior performance, both the sensing as well as catalytic, of the synthesized ZnO nanostructures are most probably due to the favourable and stable hierarchical 3D assembled architecture of single crystalline rectangular plates with exposed (100) surface, high surface area originating from high porosity of plates which are interconnected. The pores and void spaces provides increased number of active sites through amplifying the reacting surface and also facilitate the gas adsorption and desorption. Further, the network of interconnected pores offers channels for gas diffusion and mass transportation.

Conclusions

In the present work, porous rectangular ZnO plate assembled hierarchical structure is successfully synthesized using bu[l]k ZnO and aqueous ammonium carbonate, through hydrothermal treatment to hydrozincite intermediate followed by calcination, without using any organic substrate as structu[re] directing agent. Synthesized Individual plates, with 2.5-3.5µm length, 1.5 -2.5µm width and 100-150nm thickness, are single crystalline with exposed (10$\bar{1}$0) facet in flat surface. The rectangular hydrozincite plates as intermediate were formed from random thin plate by Ostwald ripening. On calcination, topotactic transformation resulted porous structure and the (100) crystal orientation of hydrozincite transformed to (100) orientation of hexagonal ZnO. The ZnO plate showed superior selective acetone sensing performance (S=3.5 in 1ppm) at 350°C. The obtained catalytic activity of synthesized ZnO plates for tetrazole synthesis is also excellent. The exhibited both the sensing and catalytic properties is superior than that [of] literature reported ZnO based materials. The synthesis of Zn[O] nanostructure from bulk ZnO in absence of any organic additive, as solvent/ structure directing agent/ surfactant makes the procedure cost effective and environment friendly. Moreover, the developed procedure is extendable for the synthesis of other doped and modified ZnO architecture.

Acknowledgements

CSIR-CSMCRI Communication No. 90/2014. The authors are thankful to the Department of Science and Technology, India (DST, SR/S1/IC-33/2011) for financial support for this work. The authors also acknowledge the Analytical Discipline and Centralized Instrument Facility of CSMCRI for materials characterization. A. K. G. acknowledges CSIR, India, for a SRF fellowship and A.S. acknowledges UGC, India, for a J[RF] fellowship. Authors also acknowledge the help of Dr. S. Neogi, CSIR-CSMCRI, for his help in crystallographic evaluation.

Notes and references

1. a) C. D. Look, *Mater. Sci. Eng. B*. 2001, **80**, 383-387; b) C. J Lee, T. J. Lee, S. C. Lyu, Y. Zhang, H. Ruh, H. J. Lee, *Appl. Phys. Lett.* 2002, **81**, 3648-3650.
2. a) J. Xu, Z. Chen, J. A. Zapien, C. S. Lee,W. Zhang, *Adv. Mater.* 2014, **26**, 5337–5367; b) H. Zhang, J. Sun, V. L. Dagle, B. Halevi, A. K. Datye, Yong Wang, *ACS Catal.* 2014, **4**, 2379−2386.
3. a) A. Sinhamahapatra, A. K. Giri, P. Pal, S. K. Pahari, H. C. Bajaj, A. B. Panda, *J. Mater. Chem.* 2012, **22**, 17227-17235; b) A. K. Giri,; A. Sinhamahapatra, S. Prakash, J. Chaudhari, V. K. Shahi, A. B. Panda, *J. Mater. Chem. A* 2013, **1**, 814-822;
4. a) C. L. Pueyo, S. Siroky, M. R. Wagner, A. Hoffmann, J. Reparaz, Lehmann, M. S. Polarz, *Adv. Funct. Mater.* 2011, **21**, 295-304.
5. a) H. Bai, Z. Liu, D. D. Sun, *Chem. Asian J.* 2012, **7**, 1771–1780; b) L. Loh, J. Briscoe, S. Dunn, *ACS Appl. Mater. Interfaces.* 2015, **7**, 152−157; c) K. Qi, J. Yang, J. Fu, G. Wang, L. Zhu, G. Liua, W. Zheng, *CrystEngComm.* 2013, **15**, 672[1]–6735; d) W. Wu, X. Xiao, T. Peng, C. Jiang *Chem. Asian J.* 2010, **5**, 315–321; e) M. Laurenti, V. Cauda, R. Gazia, M.

Fontana, V. F. Rivera, S. Bianco, G. Canavese *Eur. J. Inorg. Chem.* 2013, **9**, 2520–2527; f) S. He, L. Qiu, X. Fang, G. Guan, P. Chen, Z. Zhang, H. Peng *J. Mater. Chem. A*. 2015, **3**, 9406–9410; g) H. Dong, Z. Chen, L. Sun, W. Xie, H. H. Tan, J. Lu, C. Jagadish, X. Shen, *J. Mater. Chem.* 2010, **20**, 5510-5515; h) J. Lian, Z. Ding, F. Kwong, D. H. L. Ng, *CrystEngComm*. 2011, **13**, 4820-4822.

6. a) Z. Liu, X. D. Wen, X. L. Wu, Y. J. Gao, H. T. Chen, J. Zhu, P. K. Chu, *J. Am. Chem. Soc.* 2009, **131**, 9405–9412; b) F. Li, Y. Ding, P. Gao, X. Xin, Z. L. Wang, *Angew. Chem. Int. Ed.* 2004, **43**, 5238–5242; c) X. Liu, M. Afzaal, K. Ramasamy, P. O'Brien, J. Akhtar, *J. Am. Chem. Soc.* 2009, **131**, 15106–15107; d) Z. R. Tian, J. A. Voigt, J. Liu, B. Mckenzie, M. J. Mcdermott, M. A. Rodriguez, H. Konishi, H. Xu, *Nature Materials* 2003, **2**, 821-826; e) M. S. Mo, S. H. Lim, Y. W. Mai, R. K. Zheng, S. P. Ringer, *Adv. Mater.* 2008, **20**, 339–342.
7. Y. V. Kaneti, J. Yue, X. Jiang, J. Yu, *J. Phys. Chem. C*. 2013, **117**, 13153-13162.
8. a) X. Gao, X. Li, W. Gao, J. Qiu, X. Gan, C. Wang, X. Leng, *CrystEngComm*. 2011, **13**, 4741-4747; b) X. Cao, H, Zeng, M. Wang, X. Xu, M. Fang, S. Ji, L. Zhang, *J. Phys. Chem. C.* 2008, **112**, 5267-5270; c) J. Liu, L. Xu. B. Wei, H. Gao, X. Zhang, *CrystEngComm.* 2011, **13,** 1283-1286; d) M. H. Jung, M. J. Chu, *J. Mater. Chem. C.* 2014, **2**, 6675–6682.
9. a) J. X. Wang, C. M. L. Wu, W. S. Cheung, L. B. Luo, Z. B. He, G. D. Yuan, W. J. Zhang, C. S. Lee, S. T. Lee, *J. Phys. Chem. C*. 2010, **114**, 13157-13161; b) Z. Xing, B. Geng, X. Li, H. Jiang, C. Feng, T. Ge, *CrystEngComm.* 2011, **13**, 2137-2142; c) Y. Qiu, W. Chen, S. Yang, *J. Mater Chem.* 2010, **20**, 1001-1006; d) H. Yang, S.-Q. Ni, X. Jiang, J. Zhan, *CrystEngComm.* 2012, **14**, 6023-6028; e) L. Nasi, D. Calestani, F. Fabbri, P. Ferro, T. Besagni, P. Fedeli, F. Licci, R. Mosca, *Nanoscale* 2013, **5**, 1060-1066; f) X. Wang, W. Cai, Y. Lin. G. Wang, C. Liang, *J. Mater. Chem.* 2010, **20**, 8582-8590; g) M. Wang, B. Zhao, S. Xu, L. Lin, S. Liu, D. He, *Chem. Commun*. 2014, **50**, 930-932.
10. a) Z. Jing, J. Zhan, *Adv. Mater.* 2008, **20**, 4547-4551; b) Y. Cai, H. Fan, M. Xu, Q. Li, C. Long, *CrystEngComm*. 2013, **15**, 7339-7345; c) J. Zhang, S. Wang, M. Xu, Y. Wang, B. Zhu, S. Zhang, W. Huang, S. Wu, *Cryst. Growth Des.* 2009, **9**, 3532-3537;
11. a) X. Wang, W. Liu, J. Liu, F. Wang, J. Kong, S. Qiu, C. He, L. Luan, *ACS Appl. Mater. Interfaces* 2012, 4, 817-825; b) Y. Xiao, L. Lu, A. Zhang, Y. Zhang, L. Sun, L. Huo, F. Li, *ACS Appl Mater Interfaces.* 2012, **4**, 3797-3804; c) J. Li, H. Fan, X. Jia, *J. Phys. Chem. C*. 2010, **114**, 14684-14691; d) C. Gu, J. Huang, Y. Wu, M. Zhai, Y. Sun, J. Liu, *J. of Alloys Compd*. 2011, **509**, 4499-4504; e) Q. Qi, T. Zhang, L. Liu, X. Zheng, Q. Yu, Y. Zeng and H. Yang, *Sen. Actuators B.* 2008, **134**, 166-170; f) J. Q. He, J. Yin, D. Liu, L. X. Zhang, F. S. Cai, L. J. Bie, *Sen. Actuators B*. 2013, **182**, 170-175;
12. a) A. Mclaren, T. V. Solis, G. Li, S. C. Tsang, *J. Am. Chem. Soc.* 2009, **131**, 12540-12541; b) E. S. Jang, J. H. Won, S. J. Hwang, J. H. Choy, Adv. Mater. 2006, **18**, 3309-3312.
13. a) M. Chhowalla, H. S. Shin, G. Eda, L.-J. Li, K. P. Loh, H. Zhang, *Nat. Chem.* 2013, 5, 263-275; b) N. Sutradhar, A. K. Biswas, S. K. Pahari, B. Ganguly, A. B. Panda, *Chem. Commun.* 2014, **50**, 11529-11532; c) N. Sutradhar, S. K. Pahari, M. Jayachandran, A M. Stephan, JR Nair, B. Subramanian, H. C. Bajaj, H. M Mody, A. B. Panda, *J. Mater. Chem. A*, 2013, **1**, 9122-9131.
14. a) R. Chen, P. Zhu, T. Zhao, X. Fu, F. Zhou, R. Sun, Eur. J. *Inorg. Chem.* 2013, **20**, 3491–3496; b) T. Wang, J. Costan, A. Centeno, J. S. Pang, D. Darvill, M. P. Ryana, Fang Xie, *J. Mater. Chem. C* 2015, **3**, 2656–2663; c) C. Tamuly, I. Saikia, M. Hazarika, M. Bordoloi, N. Hussain, M. R. Dasc, K. Dekad, *RSC Adv.* 2015, **5**, 8604-8608; d) M. Umetsu, M. Mizuta, K. Tsumoto, S. Ohara, S. Takami, H. Watanabe, I. Kumagai, T. Adschiri, *Adv. Mater.* 2005, 17, 2571-2575; e) A. K. Sinha, M. Basu, M. Pradhan, S. Sarkar, T. Pal, *Chem.Eur. J.* 2010, **16**, 7865-7874; f) X. Wang, M. Liao, Y. Zhong, J. Y. Zheng, W. Tian, T. Zhai, C. Zhi, Y. Ma, J. Yao, Y. Bando, D. Golberg, *Adv. Mater*. 2012, **24**, 3421-3425; g) Z. Dong, X. Lai, J. E. Halpert, N. Yang, L. Yi, J. Zhai, D. Wang, Z. Tang, L. Jiang, *Adv. Mater.* 2012, **24**, 1046-1049; h) J. Elias, C. L. Clement, M. Bechelany, J. Michler, G. Y. Wang, Z. Wang, L. Philippe, *Adv. Mater.* 2010, **22**, 1607-1612.
15. a) L. Han, D. Wang, Y. Lu, T. Jiang, B. Liu, Y. Lin, *J. Phys. Chem. C.* 2011, **115**, 22939-22944; b) M. M. Rahman, A. Jamal, S. B. Khan, M. Faisal, *ACS Appl. Mater. Interfaces.* 2011, **3**, 1346-1351.
16. J. Liu, Z. Guo, F. Meng, T. Luo, M. Li, J. Liu, *Nanotechnology.* 2009, **20**, 125501-125508.
17. L. Wan, X. Wang, S. Yan, H. Yu, Z. Li, Z. Zou, *CrystEngComm.* 2012, **14**, 154-159.
18. B. Reeja-jayan, E. D. L. Rosa, S. S. Guzman, R.A. Rodriguez, M. J. Yacaman, *J. Phys. Chem.* 2008, **112**, 240-246.
19. S. Chakraborty, A. Sen and H. S. Maiti, Sens. Actuators B, 2006, **115**, 610-613.
20. S. Chakraborty, D. Banerjee, I. Ray and A. Sen, Current Science, 2008, **94**, 237-241.
21. (a) J. W. Mullin, *Crystallization, Butterworth Heinemann*, Boston, 4th edn, 2001; (b) X. Ge, S. Y. Song, H. J. Zhang, *CrystEngComm.* 2012, **14**, 7306-7311.
22. a) Y. Xiao, S. Liu, Feng Li, A. Zhang, J. Zhao , S. Fang, D. Jia, *Adv. Funct. Mater.* 2012, **22**, 4052–4059; b) F. Li, F. Gong, Y. Xiao, A. Zhang, J. Zhao, S. Fang, D. Jia, *ACS Nano* 2013, **7** 10482–10491.
23. F. Chen, C. Qin, Y. Cui and N. Jiao, *Angew. Chem., Int. Ed.* 2011, **50**, 11487.

Graphical Abstract

Rectangular ZnO porous nano-plate assembly with excellent acetone sensing performance and catalytic activity

Arnab Kanti Giri, Arka Saha, Aniruddha Mondal, Subhash Chandra Ghosh, Susmita Kundu, Asit Baran Panda

Assembled porous rectangular single crystalline ZnO plate, with superior acetone sensing performance and catalytic activity is presented.